RF CAVITIES AND BEAM LOADING IN THE MUON COLLIDER RECTILINEAR COOLING CHANNEL*

C. Barbagallo*, A. Grudiev, CERN, Geneva, Switzerland
D. Merenich, X. Lu[1], Northern Illinois University, DeKalb, Illinois, USA
T. Luo, Lawrence Berkeley National Laboratory, Berkeley, California, USA
[1]also at Argonne National Laboratory, Lemont, Illinois, USA

Abstract

The rectilinear cooling channel of a muon collider requires high-gradient normal-conducting RF cavities to enable ionization cooling, which is essential to achieve high luminosity. Reaching this performance demands bunches containing $\sim 10^{12}$ or even more muons in the cooling channel. At these intensities, beam-induced wakefields can cause significant beam loading, reducing the accelerating gradient and affecting beam stability. This paper presents the conceptual RF design and analysis of beam-induced effects in copper cavities designed to meet the beam dynamics requirements of the muon cooling channel. Cavities are optimized and compared in terms of RF performance and power requirements. Wakefields and beam loading are analyzed, and a compensation strategy for beam loading is proposed.

INTRODUCTION

The muon collider is a compact high-energy lepton accelerator concept aimed at advancing the frontiers of particle physics [1, 2], with a reference design targeting 10 TeV center-of-mass energy and 10 ab^{-1} integrated luminosity [3]. This requires rapid six-dimensional (6D) ionization cooling to reduce the large muon beam emittance before muon decay [4]. The International Muon Collider Collaboration (IMCC) team recently optimized the cooling lattice [5], a rectilinear channel based on the MAP concept [6] with pre-merging (Rectilinear A) and post-merging (Rectilinear B) sections, each comprising multiple identical cooling cells with absorbers, RF cavities, solenoids, and dipole magnets. The channel includes ~3,660 pillbox RF cavities operating in the TM_{010} fundamental mode (FM) at frequencies f_0 = 352–704 MHz inside multi-Tesla solenoids, and closed with beryllium (Be) windows to enhance the achievable gradient and beam transmission [7, 8]. Muon bunches of $\sim 10^{12}$ particles induce wakefields in the RF cavities, causing beam loading and a reduction of the accelerating gradient.

Guided by the latest lattice and previous Muon Ionisation Cooling Experiment (MICE) cavity designs [9–11], we designed and optimized elliptical copper (Cu) RF cavities with Be-windowed irises for each stage of the cooling channel. RF figures of merit, space-charge and resonant wakefields, and beam loading were simulated in CST Studio Suite® [12] for RF cavities with Be windows to evaluate their impact on cavity performance across the 6D cooling channel.

* work endorsed by the IMCC
* carmelo.barbagallo@cern.ch

RF CAVITY DESIGN

The RF cavity design, first presented in [13], follows the elliptical cavity parametrization of [14] (see Fig. 1). It operates in pulsed mode at 5 Hz with a duty factor of $\sim 10^{-4}$.

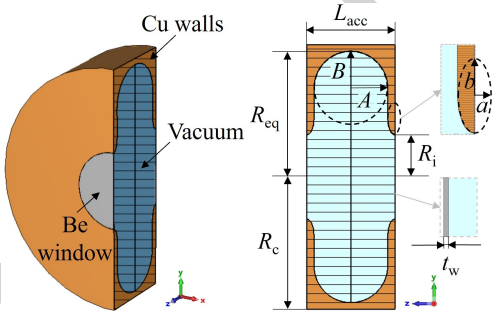

Figure 1: Single-cell RF cavity design for muon cooling [13].

Beam dynamics specifications for each stage of the cooling channel define the accelerating length L_{acc}, the nominal gradient $E_{nom} = TTF\, E_{acc}$, where E_{acc} is the accelerating gradient and TTF the transit time factor, the window radius R_i and thickness t_w (~10 µm to 120 µm depending on the stage), which are used as input for the RF cavity design. The geometrical parameters $A = B$ and the iris ellipse dimensions a and b, were optimized to minimize the peak surface electric field E_{peak} to prevent RF breakdown, while maximizing the FM shunt impedance $(R/Q) \cdot Q_0$ to reduce the surface power losses P_{diss} and the peak power $P_g = P_{diss}\beta_c$, with coupling factor $\beta_c = 1.2$. The equator radius R_{eq} tunes the cell frequency and the cavity radius is $R_c = R_{eq} + a$.

Table 1 reports the main beam dynamics inputs, the geometrical parameters, and the RF figures of merit for the single-cell cavities in the cooling channel. The geometrical shunt impedance (R/Q) is relatively stable across the different stages. The peak surface electric fields E_{peak} are below 40 MV/m, owing to an optimal E_{peak}/E_{acc} of 1.2–1.3, depending on the stage, due to the presence of the windows. Removing the windows, e.g., in the stage-B5 cavity, nearly doubles the losses and brings the E_{peak} close to 50 MV/m. The plug power of the RF system, $P_{plug,tot} = P_{g,avg,tot}/(\eta_g\, \eta_m)$, for a generator duty factor $\sim 10^{-4}$, generator efficiency $\eta_g = 0.7$, and modulator efficiency $\eta_m = 0.9$, remains within acceptable limits for pulsed normal-conducting operation.

Table 1: Single-Cell Cavity Beam Dynamics, Geometry, RF Metrics and Power Requirements for Each Cooling Stage

	Beam dynamics				Geometry			RF figures of merit of FM and power requirements											
Stage	f_0 [MHz]	L_{acc} [mm]	R_i [mm]	E_{nom} [MV/m]	A = B [mm]	a [mm]	b [mm]	R_{eq} [mm]	Q_0 [10^4]	TTF [1]	$(R/Q)(\beta)$ [Ω]	P_{diss} [MW]	$E_{peak,Cu}$ [MV/m]	$E_{peak,Be}$ [MV/m]	P_g [MW]	$N_{cell,tot}$ [1]	$P_{g,tot}$ [MW]	$P_{g,ave,tot}$ [kW]	$P_{plug,tot}$ [kW]
A1	352	190	240	27.4	75	20	44	359.08	3.05	0.906	171.73	4.24	11.72	27.38	5.09	348	1772.68	277.09	439.83
A2	352	190	160	26.4	75	20	44	359.56	3.14	0.901	149.68	4.34	23.25	26.51	5.21	356	1854.91	297.87	472.82
A3	704	95	100	31.5	37.5	10	22	180.82	2.20	0.901	160.36	2.06	20.80	31.51	2.47	405	999.42	56.70	90.00
A4	704	95	80	31.7	37.5	10	22	179.78	2.22	0.902	150.21	2.21	27.87	31.83	2.66	496	1317.10	75.41	119.70
B1	352	250	210	21.2	105	20	44	362.19	3.91	0.828	183.70	2.68	12.16	21.25	3.21	132	424.19	88.10	139.84
B2	352	220	190	21.7	90	20	44	361.56	3.56	0.864	170.47	2.81	15.25	21.76	3.37	185	623.07	130.68	207.43
B3	352	190	125	24.9	75	20	44	355.36	3.15	0.899	141.27	4.07	26.18	24.43	4.88	240	1171.61	188.80	299.68
B4	352	220	95	24.3	90	20	44	352.75	3.59	0.871	154.02	3.92	27.73	22.82	4.70	165	775.67	142.95	226.90
B5	704	95	60	22.5	37.5	10	22	177.32	2.23	0.901	140.85	1.18	24.12	22.03	1.42	275	390.14	22.37	35.51
B6	704	95	45	28.0	37.5	10	22	175.15	2.22	0.902	137.40	1.89	33.29	26.51	2.26	220	497.66	35.35	56.11
B7	704	95	38	28.5	37.5	10	22	174.04	2.22	0.904	136.87	1.97	35.25	25.98	2.36	160	378.01	23.17	36.78
B8	704	95	28	27.1	37.5	10	22	172.94	2.22	0.907	137.39	1.79	34.67	22.89	2.14	284	608.54	37.45	59.44
B9	704	95	23	29.7	37.5	10	22	172.37	2.22	0.909	138.11	2.14	38.53	23.27	2.57	208	535.13	30.57	48.52
B10	704	95	20	24.9	37.5	10	22	172.23	2.22	0.912	139.03	1.51	32.51	18.34	1.81	188	339.78	19.43	30.85

WAKEFIELDS

In the considered lattice, the muon relativistic factor β ranges from 0.88 to 0.92. In this regime, separating cavity-driven wakefields from space-charge (SC) effects is crucial. Existing wakefield solvers, such as that of CST® [12], do not provide this capability. We use a hybrid frequency–time-domain method to isolate the SC contribution from the total longitudinal wake potential:

$$W_{z,\mathrm{tot}}(t) = W_{z,\mathrm{eig}}(t) + W_{z,\mathrm{SC}}(t), \tag{1}$$

where $W_{z,\mathrm{eig}}(t)$ is the eigenmode wake potential, including the FM and higher-order modes (HOMs), and $W_{z,\mathrm{SC}}(t)$ is the SC term. The single-charge wake function is given by [15]:

$$W^0_{z,\mathrm{eig}}(t) = H(t) \sum_n \frac{\omega_n}{2} (R/Q)_n \, e^{-t/\tau_n} \cos(\omega_n t), \tag{2}$$

where $H(t)$ is the Heaviside step function, ω_n the angular frequency of mode n, $(R/Q)_n$ its geometric shunt impedance, and $\tau_n = 2Q_{\mathrm{L},n}/\omega_n$ the field decay constant, with $Q_{\mathrm{L},n}$ the loaded quality factor. The total wake potential is calculated using the CST wakefield solver for a Gaussian bunch with longitudinal length σ_z. The eigenmode wake potential is obtained by convolving $W^0_{z,\mathrm{eig}}(t)$ with the Gaussian bunch.

The SC wake potential is given by the difference between the total and eigenmode terms and can be decomposed as

$$W_{z,\mathrm{SC}}(t) = W_{z,\mathrm{ISC}}(t) + W_{z,\mathrm{DSC}}(t), \tag{3}$$

where $W_{z,\mathrm{ISC}}(t)$ is the indirect SC term generated by fields reflected from the cavity walls, and $W_{z,\mathrm{DSC}}(t)$ is the direct term from the Coulomb field [16]. To separate SC contributions, a beam-pipe (BP) model with perfect electric conductor (PEC) walls and open boundaries was simulated. In this configuration, only SC effects are present, and the longitudinal wake potential induced by a source particle on a test particle with transverse offset r_t can be written:

$$W^{\mathrm{BP}}_{z,\mathrm{SC}}(t, r_t, R_{\mathrm{BP}}) = W^{\mathrm{BP}}_{z,\mathrm{ISC}}(t, R_{\mathrm{BP}}) + W^{\mathrm{BP}}_{z,\mathrm{DSC}}(t, r_t). \tag{4}$$

The DSC term depends on r_t and scales approximately as $1/r_t^2$ [16], while the ISC term vanishes for large radii R_{BP}. This allows the cavity DSC contribution to be approximated as $W_{z,\mathrm{DSC}}(t, r_t, R_{\mathrm{eq}}) \approx W^{\mathrm{BP}}_{z,\mathrm{DSC}}(t, r_t)$ for $R_{\mathrm{eq}} \gg r_t$. Figure 2 shows the wake potential decomposition for the stage-B5 single-cell cavity with windows, together with the normalized Gaussian bunch profile. The eigenmode wake includes TM monopole modes up to a cutoff frequency determined by the bunch spectrum. Modes of higher order are neglected, as they do not contribute to the on-axis voltage [17].

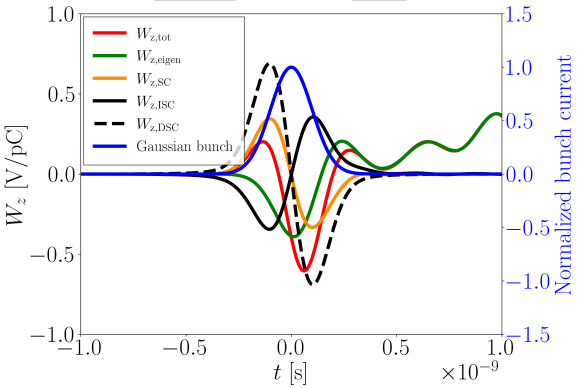

Figure 2: Wake decomposition for the stage-B5 single-cell cavity. The bunch profile is shown on the secondary axis.

In the short-range regime, the wake is dominated by SC effects, with the DSC term prevailing and the ISC smaller and opposite in sign. Both are symmetric with respect to $t = 0$ [16, 18]. In the long-range regime, the SC contribution vanishes, and eigenmodes dominate. The eigenmode wake agrees well with the total wake, validating the analytical model used for reconstruction. Similar trends are observed across cavities in each stage. The SC effects are computed for a pencil beam and are not representative of a full distribution; thus, they are not considered for beam-loading compensation. To account for the transverse dependence due to the windows, a finite transverse beam size is considered. This effect is captured by a transverse form factor:

$$F_{n,\perp}(\sigma_t) = \int_0^{R_i} 2\pi r_s \, \rho_r(r_s) \sqrt{(R/Q)_n(r_s)} \, dr_s, \tag{5}$$

where r_s is the source-particle radial position, $\rho_r(r_s)$ the normalized transverse charge density, $(R/Q)_n(r_s)$ the radial-dependent shunt impedance of mode n, and R_i the window radius. This form factor scales the wake function and, after convolution with the longitudinal bunch distribution $\lambda(t)$, yields the finite-beam eigenmode wake potential:

$$W_{z,\mathrm{eig}}^{\mathrm{finite}}(t) = \frac{1}{Q_b}\int_{-\infty}^{t} F_{n,\perp}(\sigma_t) W_{z,\mathrm{eig}}^{0}(t-t')\lambda(t')\,dt', \quad (6)$$

where $\sigma_t = R_i/3$ [19] is the transverse beam size and Q_b the bunch charge. The longitudinal eigenmode wake potential obtained from the analytical model is in good agreement with the results from CST PIC simulations (see Fig. 3).

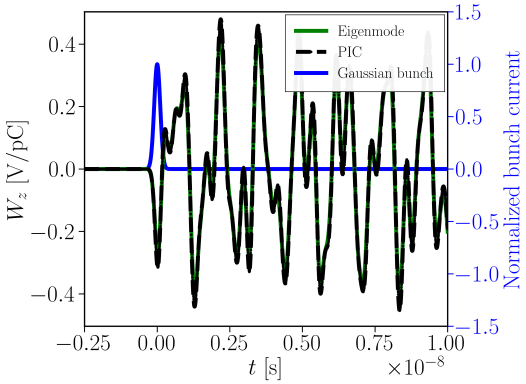

Figure 3: Comparison of the analytical and PIC longitudinal wake potentials for the stage-B5 single-cell cavity.

BEAM LOADING

Beam loading modifies both the amplitude and the local slope of the RF voltage seen by the bunch. If uncompensated, it can lead to longitudinal emittance growth and energy spread [20]. To mitigate these effects, a local compensation scheme is applied at the bunch center ($t = 0$):

$$\begin{cases} V_{\mathrm{RF}}(t) + V_b(t) = V_{\mathrm{RF,L}}(t) \\ \dfrac{\partial V_{\mathrm{RF}}(t)}{\partial t} + \dfrac{\partial V_b(t)}{\partial t} = \dfrac{\partial V_{\mathrm{RF,L}}(t)}{\partial t} \end{cases} \quad \text{at } t = 0, \quad (7)$$

where $V_{\mathrm{RF}}(t) = V_{\mathrm{RF,acc}}(t) + V_{\mathrm{RF,foc}}(t)$ is the applied RF voltage, $V_b(t)$ the beam-induced voltage, and $V_{\mathrm{RF,L}}(t)$ the desired loaded RF voltage. The accelerating component $V_{\mathrm{RF,acc}}(t)$ is adjusted to cancel $V_b(t)$ at $t = 0$, while the focusing component $V_{\mathrm{RF,foc}}(t)$ restores the required voltage slope. This preserves a linear voltage profile around $t = 0$, mitigating energy spread. Only FM and HOM contributions were compensated, as they allow for linear compensation. The effect of beam loading and its compensation in the stage-B5 multi-cell cavity is illustrated in Fig. 4.

Table 2 reports the main RF figures of merit after beam loading compensation for the multi-cell cavities with Be windows at each stage of the cooling channel. Voltage and power values divided by the number of cavity cells N_{cell} give single-cell equivalents. Beam-loading compensation is found to increase the RF voltage by up to a factor of two, resulting in higher peak surface fields than in the uncompensated case.

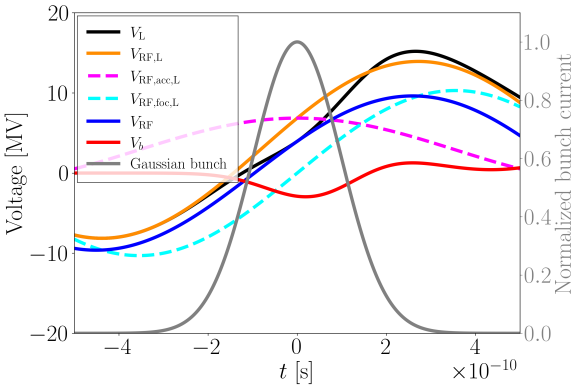

Figure 4: Beam loading in the stage-B5 multi-cell cavity.

Table 2: RF Figures of Merit After Beam-Loading Compensation for Multi-Cell Cavities With Be Windows

Stage	β [1]	σ_z [mm]	Q_b [μC]	N_{cell} [1]	$V_{\mathrm{RF},0}$ [MV]	$\lvert V_{b,0}\rvert$ [MV]	$V_{\mathrm{RF,L},0}$ [MV]	P'_{diss} [MW]	$E'_{\mathrm{peak,Cu}}$ [MV/m]	$E'_{\mathrm{peak,Be}}$ [MV/m]
A1	0.92	95.44	0.37	6	28.31	2.72	32.44	33.44	13.43	31.37
A2	0.89	59.51	0.28	4	18.07	2.48	22.69	27.38	29.19	33.28
A3	0.89	32.97	0.23	5	13.47	4.61	13.75	10.70	21.22	32.14
A4	0.901	22.41	0.19	4	10.87	5.44	22.32	37.32	57.23	65.36
B1	0.886	56.58	2.98	6	26.32	2.22	30.59	21.71	14.14	24.70
B2	0.885	57.05	2.54	5	20.62	1.49	23.38	18.03	17.29	24.66
B3	0.887	41.22	2.27	4	17.01	1.53	20.45	23.52	31.47	29.37
B4	0.886	36.13	1.98	3	13.97	1.18	16.80	17.00	33.35	27.45
B5	0.889	27.71	1.78	5	9.63	1.96	13.28	11.26	33.28	30.40
B6	0.888	23.64	1.59	4	9.60	1.60	12.88	13.56	44.64	35.56
B7	0.887	21.81	1.41	4	9.79	1.48	13.11	14.12	47.20	34.79
B8	0.884	20.97	1.31	4	9.34	1.35	12.58	12.95	46.69	30.82
B9	0.881	19.60	1.15	4	10.26	1.25	13.47	14.79	50.60	30.56
B10	0.884	19.64	0.98	4	8.63	1.07	11.39	10.51	42.94	24.23

CONCLUSION

This work presented the RF design and beam-loading analysis of Cu cavities for the muon collider rectilinear cooling channel. Be-windowed cavities are essential to achieve acceptable RF performance. Wakefields and beam-loading effects were analyzed. An analytical model including a finite transverse beam size was developed to capture the transverse dependence introduced by the windows and was validated against PIC simulations. Beam loading was locally compensated around the bunch center by canceling the beam-induced voltage and restoring the required voltage slope. These results provide design guidelines for RF systems in the cooling channel. Full beam dynamics studies are required to assess the impact of beam loading and its compensation on channel performance.

ACKNOWLEDGEMENTS

Funded by the European Union. The views expressed are those of the authors and do not necessarily reflect those of the EU or the European Research Executive Agency, which are not responsible for them. The authors acknowledge U.S. DOE Office of Science support (Awards DE-SC0014664, DE-SC0021928, and Contract DE-AC02-05CH11231).

REFERENCES

[1] K. R. Long *et al.*, "Muon colliders to expand frontiers of particle physics", *Nature Phys.*, vol. 17, no. 3, p. 289–292, 2021. doi:10.1038/s41567-020-01130-x

[2] C. Accettura *et al.*, "The Muon Collider", CERN Report CERN-ACC-2025-001, to be published, arXiv:2504.21417. doi:10.48550/arXiv.2504.21417

[3] C. Accettura *et al.*, "Towards a muon collider", *Eur. Phys. J. C*, vol. 83, no. 864, 2023. doi:10.1140/epjc/s10052-023-11889-x

[4] D. Neuffer, "Introduction to muon cooling", *Nucl. Instrum. Methods Phys. Res. Sect. A*, vol. 532, p. 26–31, 2004. doi:10.1016/j.nima.2004.06.051

[5] R. Zhu *et al.*, "Design method, performance evaluation, and tolerance analysis of the rectilinear cooling channel for a muon collider", *Phys. Rev. Accel. Beams*, vol. 28, p. 041003, 2025. doi:10.1103/PhysRevAccelBeams.28.041003

[6] D. Stratakis and R. B. Palmer, "Rectilinear six-dimensional ionization cooling channel for a muon collider: A theoretical and numerical study", *Phys. Rev. Spec. Top. Accel. Beams*, vol. 18, p. 031003, 2015. doi:10.1103/PhysRevSTAB.18.031003

[7] D. Bowring *et al.*, "Operation of normal-conducting RF cavities in multi-tesla magnetic fields for muon ionization cooling: A feasibility demonstration", *Phys. Rev. Accel. Beams*, vol. 23, p. 072001, 2020. doi:10.1103/PhysRevAccelBeams.23.072001

[8] D. Li, "High power RF test of an 805 MHz RF cavity for a muon cooling channel", in *Proc. EPAC'02*, Paris, France, 2002, pp. 2160–2162. https://cds.cern.ch/record/584750

[9] D. Li *et al.*, "Design and fabrication of an 805 MHz RF cavity with Be windows for high-power testing in a muon cooling experiment", in *Proc. PAC'01*, Chicago, IL, USA, 2001, vol. 2, pp. 918–920. doi:10.1109/PAC.2001.986524

[10] D. Li *et al.*, "Progress on the RF coupling coil module design for the MICE channel", in *Proc. PAC'05*, Knoxville, TN, USA, 2005, pp. 2869–2871. doi:10.1109/PAC.2005.1591297

[11] D. Li *et al.*, "201 MHz cavity R&D for MuCool and MICE", in *Proc. EPAC'06*, Edinburgh, Scotland, 2006, p. 1391. https://www.osti.gov/servlets/purl/889262

[12] Computer Simulation Technology, *CST Studio Suite 2024*. https://www.3ds.com/products/simulia/cst-studio-suite

[13] C. Barbagallo and A. Grudiev, "Conceptual RF design and modelling of a 704 MHz cavity for the muon cooling complex", in *Proc. IPAC'24*, Nashville, TN, USA, 2024, pp. 2532–2535. doi:10.18429/JACoW-IPAC2024-WEPR25

[14] V. Shemelin, "Optimal choice of cell geometry for a multicell superconducting cavity", *Phys. Rev. Spec. Top. Accel. Beams*, vol. 12, p. 114701, 2009. doi:10.1103/PhysRevSTAB.12.114701

[15] P. B. Wilson, "Introduction to Wake Fields and Wake Potentials", in *Proc. AIP Conf.*, no. 184, pp. 525–564, 1989. doi:10.1063/1.38045

[16] K. Schindl, "Space charge", CERN Report CERN-PS-99-012-DI, 1999. https://cds.cern.ch/record/2849995

[17] S.-H. Kim *et al.*, "Higher-order-mode (HOM) power in elliptical superconducting cavities for intense pulsed proton accelerators", *Nucl. Instrum. Methods Phys. Res. Sect. A*, vol. 492, pp. 1-10, 2002. doi:10.1016/S0168-9002(02)01286-X

[18] N. Mounet *et al.*, "Closed-form formulas of the indirect space-charge wake function for axisymmetric structures", in *Proc. HB'21*, East Lansing, MI, USA, 2021, pp. 65-70. doi:10.18429/JACoW-HB2021-MOP10

[19] C. Rogers, private communication, November 2023.

[20] T. P. Wangler, *RF Linear Accelerators*, 2nd ed., Wiley, New York, 2008.